Hydrodynamic Tests on a Fixed Plate in Uniform Flow

K. Klaka[1], J.D. Penrose[1] , R.R Horsley[1] and M.R. Renilson[2]

[1]Centre for Marine Science and Technology

Curtin University of Technology, Perth, Western Australia, 6102

AUSTRALIA

fax: (61) 8 9266 4799 email: k.klaka@curtin.edu.au

[2]Centre for Marine Technology, QinetiQ, Gosport, PO12 2AG, UK

ABSTRACT

The forces and moments acting on a vertical flat plate in open flow running normal to the surface of the plate have been subject to investigation for several decades. However, the forces and moments acting on surface piercing plates, plates slightly inclined to the vertical and plates extending close to a lower boundary have not received such attention. A series of experiments was conducted as part an investigation into the hydrodynamics of sailing yacht keels, with particular application to the case of a yacht drifting laterally down stream. The results may be of value for a wider range of engineering problems involving the flow of water over surface-piercing plates.

It was found that drag force and heel moment varied approximately as flow speed squared for all plates investigated; the influence of plate angle on drag coefficient was small, with no clear trend; the magnitude of the drag coefficients for the surface-piercing plates was greater than for published data on fully submerged plates; and the centre of pressure was at approximately 50% of the span. The data scatter at low Froude numbers restricts the validity of these conclusions to Froude numbers greater than 0.1.

KEYWORDS

Hydrodynamics, free-surface flow, vortical flow, open channel flow

NOMENCLATURE

A profile area of plate when vertical (m^2)

C_p centre of pressure (dimensionless)

C_d drag coefficient (dimensionless)

C_φ heel moment coefficient (dimensionless)

D water depth (m)

F_d drag (N)

Fn Froude number (dimensionless)

g acceleration due to gravity ($m\ s^{-2}$)

k_1 constant of proportionality

M_φ roll moment (Nm)

n exponent (dimensionless)

Re Reynolds number (dimensionless)

s span (m)

u flow velocity ($m\ s^{-1}$)

ν kinematic viscosity ($m^2\ s^{-1}$)

ρ density ($kg\ m^{-3}$)

1 BACKGROUND

Open channel flows have been studied extensively with obstructions emanating from the channel floor [1], [2], but few data exist for surface-suspended obstructions. Studies have been conducted on the flow under a gate [3] p.180 for flows with substantially different water levels either side of the gate, where hydraulic jumps may occur. Most work on such objects focussed on water depth and velocity changes rather

than the forces exerted on the plate. One of the few relevant data sets was that of Hay, reported in [4] p10-15. This showed the drag coefficient of a surface piercing flat plate normal to the flow as a function of plate-depth based Froude number, for a range of plate aspect ratios.

The experiments described in this paper were conducted as part of a project investigating the hydrodynamics of sailing yacht keels. The aim of the test program was to measure the hydrodynamic drag and heel moment acting on flat plates at near-normal angles to the flow. Variables investigated were flow speed, plate angle and plate aspect ratio. The proposed experiment was intended to extend the very limited data set for the forces on surface piercing flat plates at near-normal angles to uniform flow.

A right handed axes convention was used (Figure 1), with the origin at the still water level, at mid-chord and mid-thickness. The positive y-direction was downstream, positive z-direction was up and consequently positive (clockwise) heel angle was with the plate tip downstream of the hinge. The heel moment was also positive in a clockwise direction.

The chord was defined as the dimension across the plate, which represented the heading of the yacht when the yacht was sailing. The span was the length of the plate when vertical, normal to the flow orthogonal to the chord. The thickness of the plate was the dimension in line with the flow when the plate was vertical. The plate aspect ratio for the rectangular plates used in this experiment was the ratio of span to chord.

Drag is the force horizontal component parallel to the flow direction. Lift is the vertical component normal to the flow direction.

The torque generated by the total force about the static water level is called the heel moment. For the conditions of these experiments the lift force contribution to heel

moment was at least one order of magnitude less than that from the drag, so was not included.

2 METHODOLOGY

2.1 Parameter space

Three plate aspect ratios were investigated (Figure 2 and Table 1):

- a full width rectangular flat plate with 3mm clearance at the ends, of geometric aspect ratio 0.143, but zero effective aspect ratio (plate a).
- a half depth rectangular flat plate of aspect ratio 0.91 (plate b).
- a full depth rectangular flat plate of aspect ratio 4.4 (plate c). With the plate vertical, the tip of the plate was 5mm from the channel bed.

The latter two plate geometries were representative of the aspect ratios of yacht appendages, which provided the primary motivation for the investigation.

The flow speeds available were such that the depth-based Froude number was always less than unity i.e. the sub-critical range.

Plate angles ranged from +15° to –15°; over this range the plate could reasonably be expected to exhibit fully separated flow. Flow velocities ranged from $0.1 ms^{-1}$ to $0.6 ms^{-1}$, yielding span-based Reynolds numbers from 0.42×10^4 to 1.2×10^5.

These experimental conditions are representative of the flow over a yacht appendage drifting beam on to waves or current, and the flow past the rudder on a vessel undertaking an extreme turning manoeuvre with full helm applied.

2.2 Scaling

The plate forces are a function of both Froude number (*Fn*):

$$Fn = \frac{u}{\sqrt{gD}} \quad (1)$$

where u is the flow velocity, g is the acceleration due to gravity and D is the water depth,

and Reynolds number (Re):

$$Re = \frac{u\ s}{\nu} \quad (2)$$

where ν is the kinematic viscosity and s is the plate span.

Drag and heel moment were non-dimensionalised as follows:

$$C_d = \frac{F_d}{\frac{1}{2}\rho A u^2} \quad (3)$$

$$C_\varphi = \frac{M_\varphi}{\frac{1}{2}\rho A u^2 s} \quad (4)$$

where A is the plate profile area when vertical, C_d is the drag coefficient, C_φ is the heel moment coefficient, F_d is the drag, M_φ is the roll moment, s is the plate span, u is the flow velocity and ρ is the water density. Under Froude scaling the inertial effects would be correctly scaled. The Reynolds number would change but the effects are usually quite small if there is a significant amount of separated flow and the separation points do not change with Reynolds number [4], [5]. In such circumstances the non-dimensionalised forces and moments may be compared directly for experiments conducted at the same Froude number. Nevertheless care should be taken when comparing results from experiments conducted at significantly different Reynolds number. Furthermore caution is urged to check that the non-dimensionalising parameters used are the same.

2.3 Blockage

An object placed in a channel will experience different forces compared with the same object placed in unrestricted flow. This effect is known as blockage and is reasonably well understood for wind tunnel and towing tank experiments [6], [7]. However, wind tunnel blockage corrections do not apply to tests with a pressure-relieving free surface, and towing tank blockage corrections are largely focussed on surface wave effects and small ratios of model cross sectional area to tank cross sectional area. The conditions of the experiment described in this paper lie outside the range of object slenderness and channel aspect ratio for which empirical towing tank blockage formulae have been developed. Channel aspect ratio is surprisingly important, as shown in the first data subset of table 1 in [7]. The free surface channel wall interference effects may be calculated using potential flow theory. Numerous investigations on wall interference have been carried out for relatively slender shapes that generate Kelvin wave patterns [8], [9]. The flat plates in the experiments described in this paper were not slender and generated wide viscous wakes which would have strong interactions with the generated and reflected wave fields.

The results have been presented in uncorrected form, given the dependence of the result on the method adopted. This makes the data more useful to other researchers who may apply their preferred blockage correction. This should be borne in mind when comparing with experiments conducted in facilities with different ratios of plate area to channel cross sectional area.

3 EQUIPMENT

The facility was a circulating open water channel, with a 10m long working length of cross section 300mm square. The water was circulated using a centrifugal pump. The flow rate (and in consequence, the water depth) was regulated by a flow valve. The water depth can be controlled separately by changing the height of a sluice gate at the downstream end.

The plates were made of 6mm Perspex with square edges. The plate dimensions are shown in Table 1. The attachment rig for holding the plates comprised two horizontal aluminium bases connected by vertical rods (Figure 3 and Figure 4). The upper base was clamped to the sides of the channel. The hinge supports, crank and crank arm were attached to the lower base. The angle of the plate was adjusted via the crank arm by rotating a motor (not powered for these experiments). The hinge supports could be adjusted so that the hinge line was always at the calm water level.

The instrumentation for these experiments comprised twelve strain gauges and a Pygmy 30mm diameter flow meter to measure flow rate. The strain gauges were calibrated statically by applying known loads to each hinge support and the crank arm connection, for a number of directions over a range of amplitudes. The mean value of the gauges over typically 5 seconds was recorded. These mean values were plotted and a linear regression of load against voltage performed in order to determine the calibration factor. Cross-axis sensitivity of the gauges was measured during calibration and showed that measured strains were parallel to the plane of the tank.

Water depth was measured using steel rules permanently mounted on the outside of the channel. All signals acquired were analogue voltages, digitised at 100Hz with anti-aliasing filters set at 20Hz.

4 PROCEDURE

The strain gauge circuits were allowed to warm up for typically one hour in order to reduce gauge drift due to temperature variation. The procedure for each run was to set the plate angle by adjusting the motor crank. The angle was measured using an adjustable square. The channel was then filled with water to the correct depth and approximate desired flow speed. This required adjustment of both the flow valve and sluice gate until an appropriate flow speed was attained at a steady state.

On completion of sampling, the flow speed was measured at six transverse locations at a plane 200mm ahead of the plate and represented the region of the plane occupied by the plate and not the region affected by the channel wall boundary layer. On completion of a test run the sluice gate and valve were adjusted for the next flow speed. Before and after each series of flow speeds, a static calibration run in air was conducted. These runs served as the zero datum for the gauge signals.

The plates were always set with the hinges at the static waterline. All tests were conducted at a water depth of 0.205m.

An acquisition time of 20 seconds was used for each run. The mean values of every signal were zero-subtracted from their nearest (in time) in-air run. The gauge calibration factors were then applied, and the total drag and heel moment determined from the individual gauges. The heel moment was determined by taking moments about the hinge support. The static moment component due to buoyancy (not present in the zero datum in-air runs) was calculated analytically then subtracted from the total heel moment. The hinge support tare was subtracted from the calculated forces and moments. A power law line of best-fit plot of force as a function of flow velocity revealed an offset on the y-axis which was removed by subtracting the offset of the best

fit line from each data point. This step was important for the final processing stage – the conversion of forces and moment to dimensionless coefficients – because the denominator contained a velocity squared term which would have introduced large errors at low flow speeds if the zero velocity offset was not removed.

5 ERRORS

The sizes of the rig components were small relative to the size of the gauges, so there were errors due to strain gradients, gauge thickness etc. However, these were largely accounted for in the calibration process. Temperature effects were accounted for in two ways; firstly, by choosing gauges with a thermal expansion coefficient similar to that of the attachment plate; secondly, by taking measurements over short duration, which were thus unlikely to experience significant change in temperature in such a large body of water. The specifications of the gauges were such that changes in signal due to thermal effects were less than 0.1%. Errors were calculated from the signal standard deviation for the run. Calibration errors were estimated from the standard deviations of the time series of the calibration signals. The coefficient of determination (r^2) for the calibration factors was always greater than 0.999. Errors for the in-air datum signal were estimated from the standard deviation of the datum readings over a day's testing at uniform gain setting. Tare errors were estimated as the same as for a low speed flow run. The errors from these sources were propagated through to the forces and moments. The errors in the flow velocity were determined from the standard deviation of the spatial measurements. Errors due to time variation of velocity were not independent of the errors in the time series of the gauge signals, so were not estimated separately. The velocity error estimate, and those of the other denominators in the non-dimensional

coefficients, were then propagated to yield errors in the coefficients. Errors in the correction for buoyancy-induced moment introduced errors in the heeling moment coefficient except for when the plate angle was zero. For the worst case of plate a at 15° heel angle the buoyancy correction amounted to 20% of the total moment at low Froude number, decreasing to 5% at high Froude number. An error is present in that the buoyancy calculation was determined assuming the static water level, whereas there was a step in the water level which increased in size with increasing Froude number. However, the step was distributed either side of the static water level, and the worst case error due to the buoyancy correction when propagated to the heeling moment is 2%, generally far less. The buoyancy correction has no influence on the drag . A summary of error magnitudes for drag is given in Table 2; heel moment errors were of similar proportion.

It was clear from the error propagation process that the relative values of the errors were greatest at lower flow speeds because the amplitude of the zero datum and tare corrections were then of the same order as the uniform flow signal. The largest source of error for most conditions was from the zero datum. Flow velocity and plate immersed area errors were also significant. The errors in instrument calibration were two orders of magnitude less than other error sources. Error bars shown in the figures are 90% confidence limits, calculated assuming a normal distribution. The envelope of the confidence limits for the designated data set is shown by dotted lines. The confidence limits for only a single data set on each graph are shown for clarity.

6 RESULTS AND DISCUSSION

Figure 5, Figure 6 and Figure 7 show the drag coefficient as a function of Froude number for the three plates tested. It is noted that the large error bars at low Froude number restrict meaningful discussion to phenomena occurring at Froude numbers greater than 0.1.

It is evident from these figures that the drag coefficient varies with Froude number. In order to illustrate the effect more closely, the best-fit values of the speed exponent n in the drag-velocity equation (5) were calculated and are shown in Figure 8.

$$F_d = k_1 u^n \qquad (5)$$

Where F_d is drag, k_1 is a constant of proportionality, u is flow velocity and n is an exponent.

The mean value of the exponent for all conditions was 2.07, with a range of 1.76 to 2.41 (with one outlier at 1.15). If there were no Reynolds number, blockage or free surface effects, the exponent would be expected to hold a value of 2. The small variation from this figure implies that such effects are relatively modest. However, the value of the exponent for plate b is consistently greater than that for the other two plates.

The magnitude of the drag coefficient was in the region 1.5 to 2.3, somewhat higher than the value of 1.2 for a plate normal to the flow in an unconfined flow [9]. The difference is probably due to a combination of blockage and free surface effects. The free surface effect would be expected to increase with Froude number, as evidenced by Hay in Hoerner [4] p10-15. The maximum drag coefficient found by Hay was 1.6, occurring at Froude numbers greater than 1. Hoerner considered these high values to be a consequence of wave drag. The free surface distortion in the current experiments

(measured by the change in water level across the plate thickness) supported this hypothesis, but the low dependence of drag coefficient from Froude number implies either a false hypothesis or some other effect counteracting the wave drag increase – possibly a free-surface blockage change.

Figure 9 shows the variation of the drag coefficient as a function of plate angle. The effect of plate angle on drag was small. This is in accordance with results for circular cylinders inclined to the flow [10].

Figure 10 shows the variation of drag coefficient with Froude number for each plate. Plate a and plate b exhibit similar drag coefficients, despite plate a extending across the channel with only a 3mm gap at each end. Conversely, plate c had a higher drag coefficient than either plate a or plate b. This may have been due to the very small tip clearance from the channel bed for plate c – less than 5mm - restricting the flow.

Heel moment variation followed generally similar trends to that for drag. An example is shown in Figure 11. The corresponding power law dependency is shown in Figure 12, the mean value of the exponent being 1.91.

The spanwise centre of pressure was estimated from the ratio of heel moment to drag force. This did not take account of lift force, but the contribution of lift to heel moment was small over the range of heel angles tested. The results for 0° heel angle (at which the lift influence was zero) are shown in Figure 13. The position of the centre of pressure was close to 50% of plate span below the static water level for plates a and b, as might be expected for a fully immersed plate. This suggests that the effect of the free surface on force generation was either small, or uniform down the span of the plate. The centre of pressure was slightly closer to the surface for plate c. The effect on centre of pressure of the small tip clearance of plate c was also very small.

7 CONCLUSIONS

For the plates used in the experiment, at Froude numbers between 0.1 and 0.4 and plate angle range +20° to -15°, the following conclusions were drawn:

- Drag force and heel moment varied approximately as flow speed squared for all plates investigated.
- The influence of plate angle on drag coefficient was small, with no clear trend.
- The magnitude of the drag coefficients for the surface-piercing plates was greater than for published data on fully submerged plates.
- The centre of pressure was at approximately 50% of the span.

8 REFERENCES

[1] N. B. Webber, Fluid mechanics for civil engineers, Chapman & Hall, London, 1971.

[2] B. S. Massey, Mechanics of fluids, Van Nostrand Reinhold, 1979.

[3] M. H. Chaudhry, Open-channel flow, Prentice Hall, New Jersey, 1993.

[4] S. F. Hoerner, Fluid dynamic drag, Hoerner Fluid Dynamics, Bricktown USA, 1965.

[5] S. F. Hoerner and H. V. Borst, Fluid dynamic lift, Hoerner Fluid Dynamics, Bricktown, USA, 1975.

[6] W. H. Rae and A. Pope, Low-speed wind tunnel testing, John Wiley & Sons, 1984.

[7] J. R. Scott, Blockage correction at sub-critical speeds, Transactions Royal Institution of Naval Architects 118 (1976) 169-179.

[8] J. Xia and J. R. Krokstad, Wave forces on a body in confined waters, 14th Australasian Fluid Mechanics Conference, Adelaide, 10-14 December 2001, 6.

[9] J. N. Newman, Marine hydrodynamics, MIT Press, Cambridge Massachusetts, 1977.

[10] V. Sundar, V. Vengatesan, G. Anandkumar and A. Schlenkhoff, Hydrodynamic coefficients for inclined cylinders, Ocean Engineering 25 4-5 (1998) 277-294.

	Plate a	Plate b	Plate c
mass (kg)	0.105	0.075	0.069
Immersed span (m)	0.042	0.091	0.20
Chord (m)	0.294	0.10	0.0455
Area (m^2)	0.0123	0.0091	0.0091
Geometric aspect ratio	0.143	0.91	4.4

Table 1 Plate geometry

	Low speed (*Fn* =0.161)		**High speed** (*Fn* = 0.364)	
	Standard deviation	mean	Standard deviation.	mean
drag (N)	0.031	0.11	0.064	1.9
C_d	0.33	1.29	0.05	1.72

Table 2 Error estimates: plate a, 10° angle

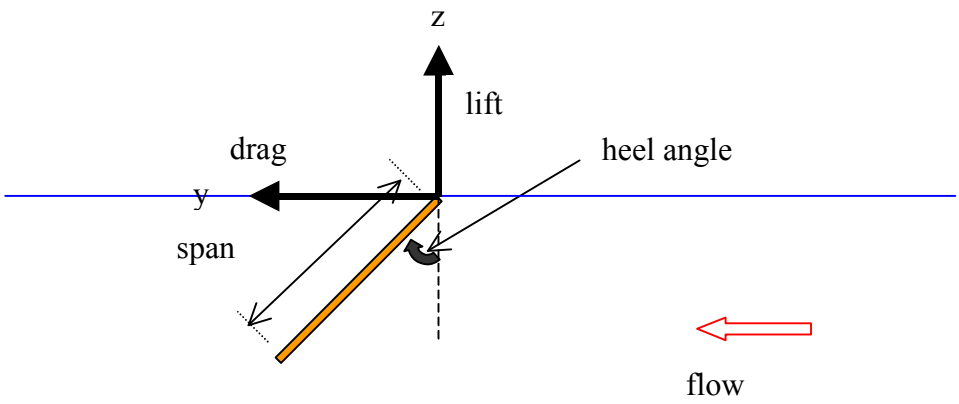

Figure 1 Definition of forces

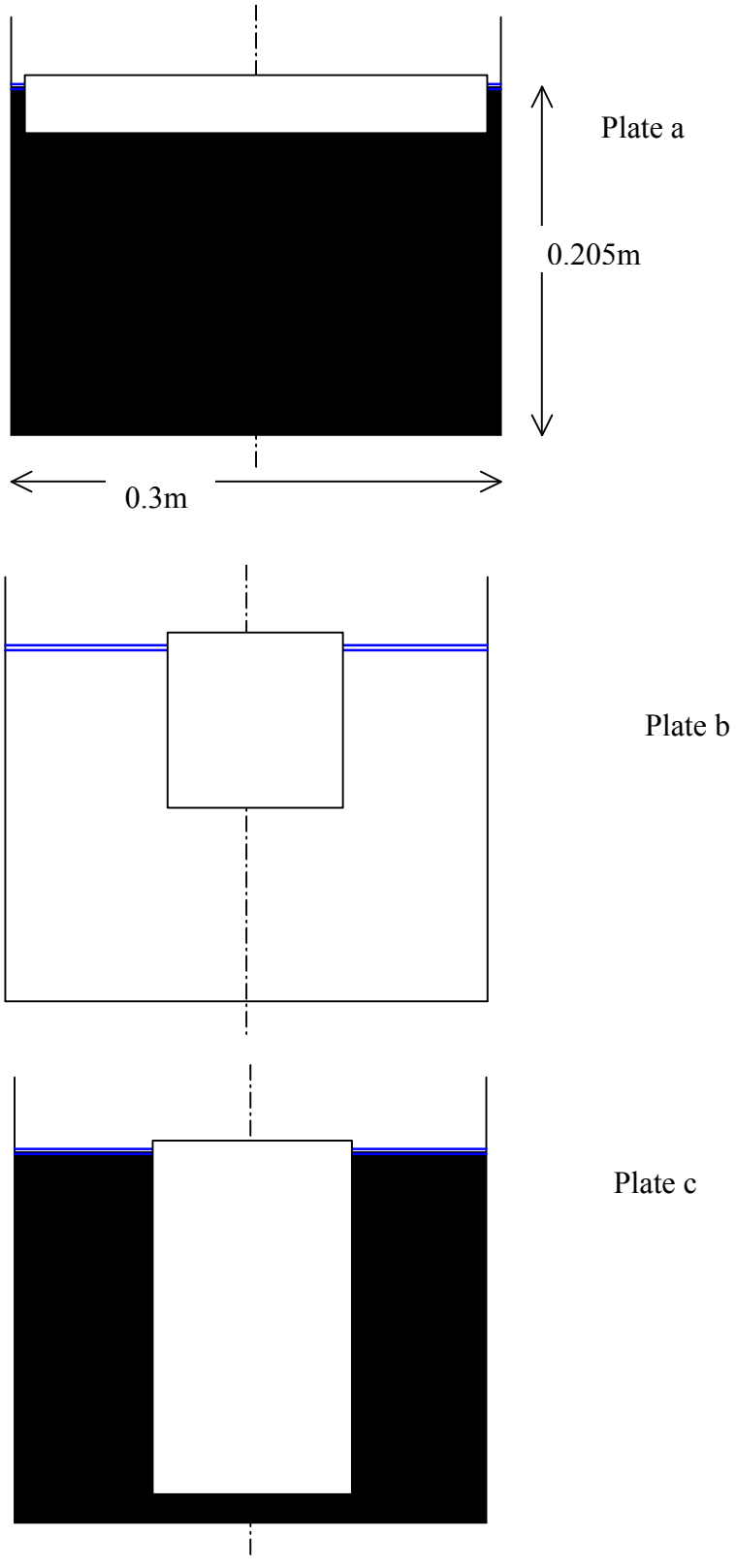

Figure 2 Plate geometry

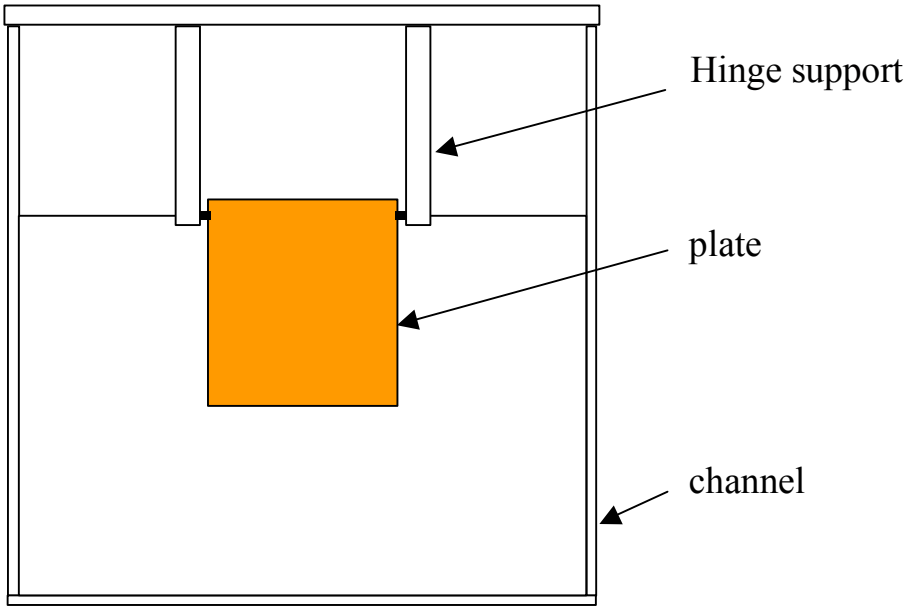

Figure 3 Experimental rig: end view

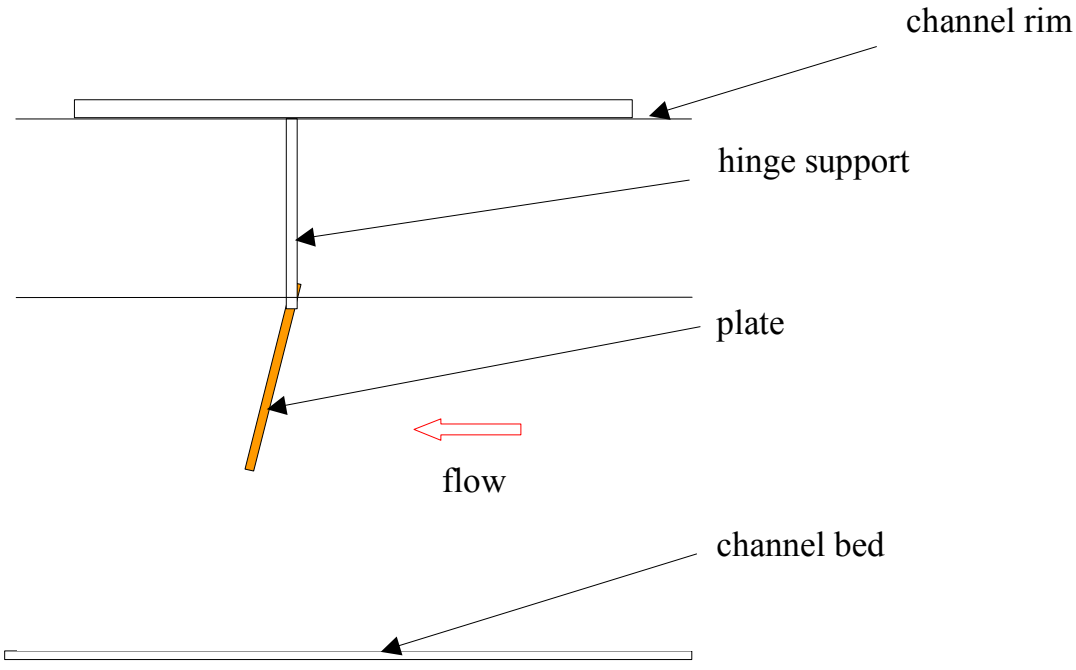

Figure 4 Experimental rig: side view

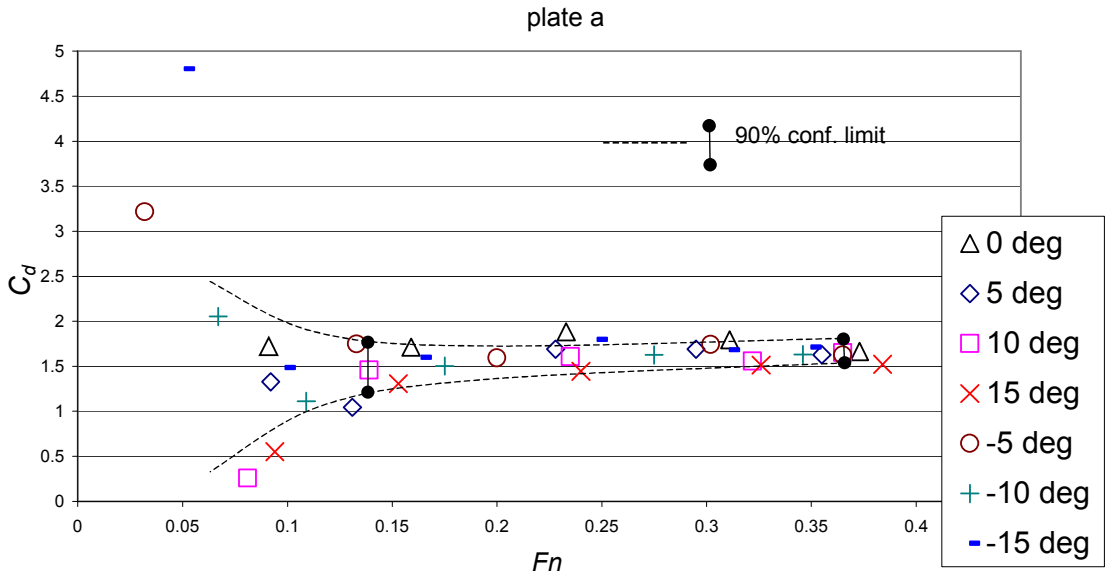

Figure 5 Drag coefficient as a function of Froude number; plate a

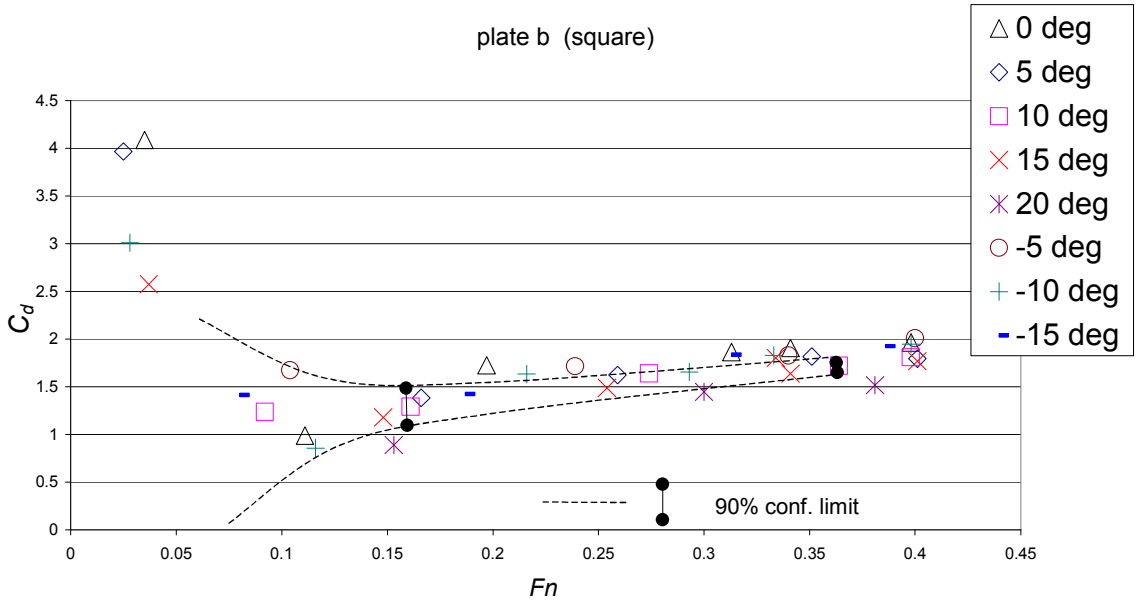

Figure 6 Drag coefficient as a function of Froude number; plate b

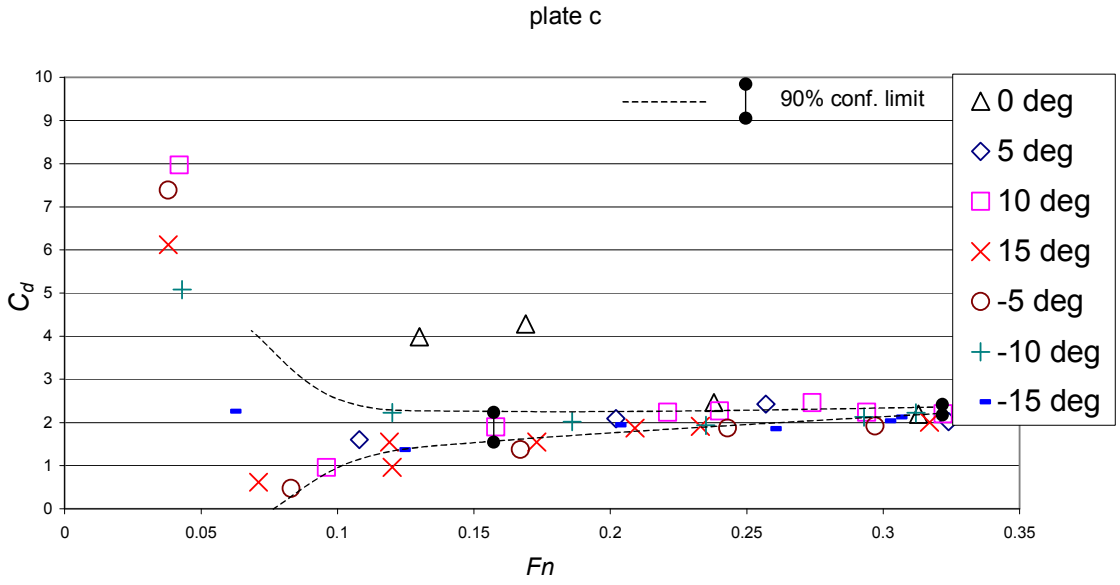

Figure 7 Drag coefficient as a function of Froude number; plate c

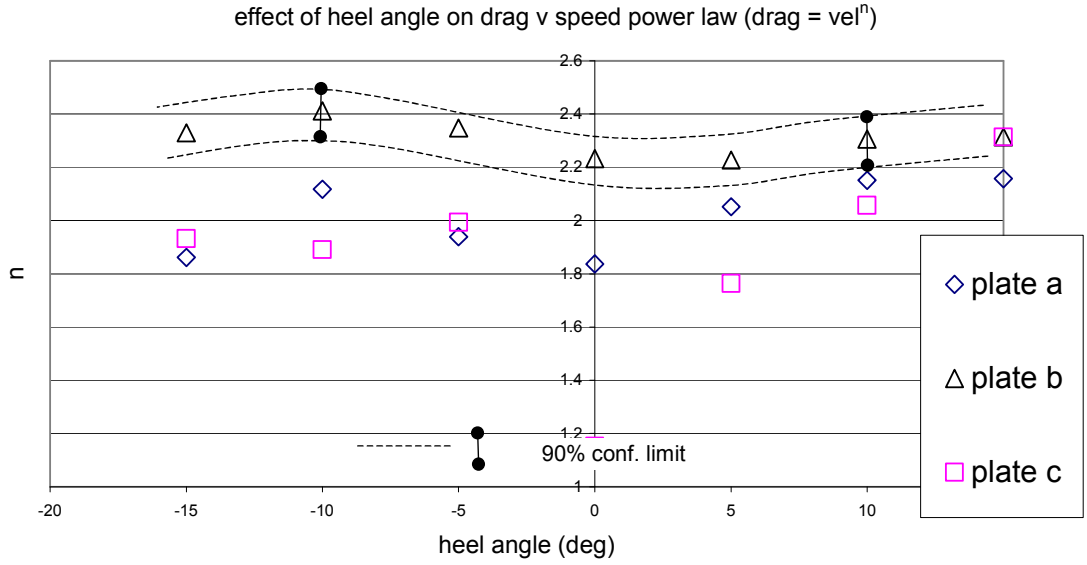

Figure 8 Power law variation with angle and plate geometry

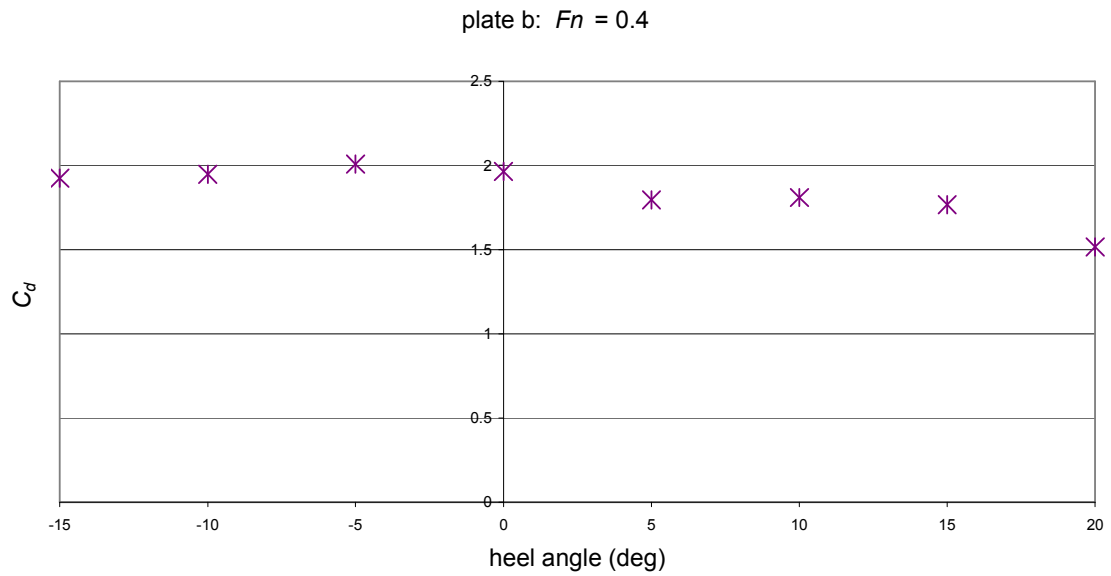

Figure 9 Effect of plate angle on drag, plate b Froude no. = 0.4

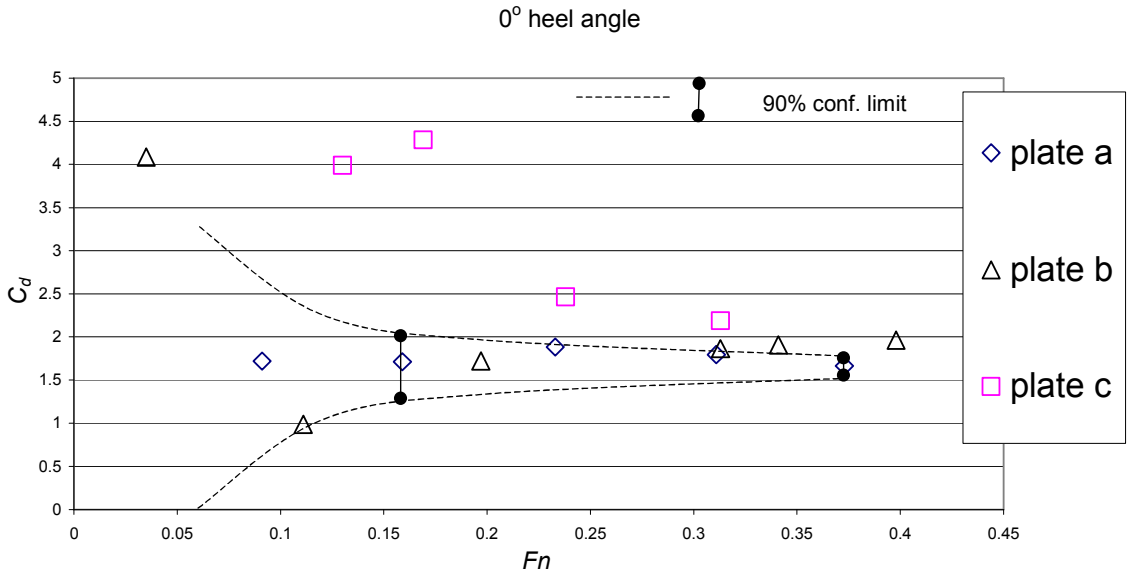

Figure 10 Effect of plate geometry on drag coefficient

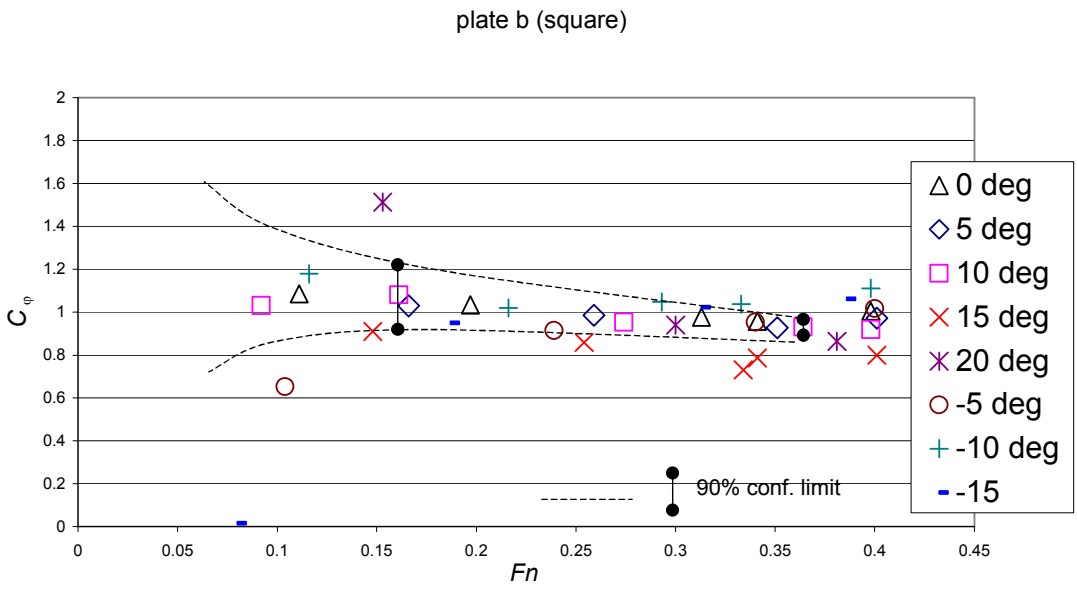

Figure 11 Variation of heel moment coefficient for plate b

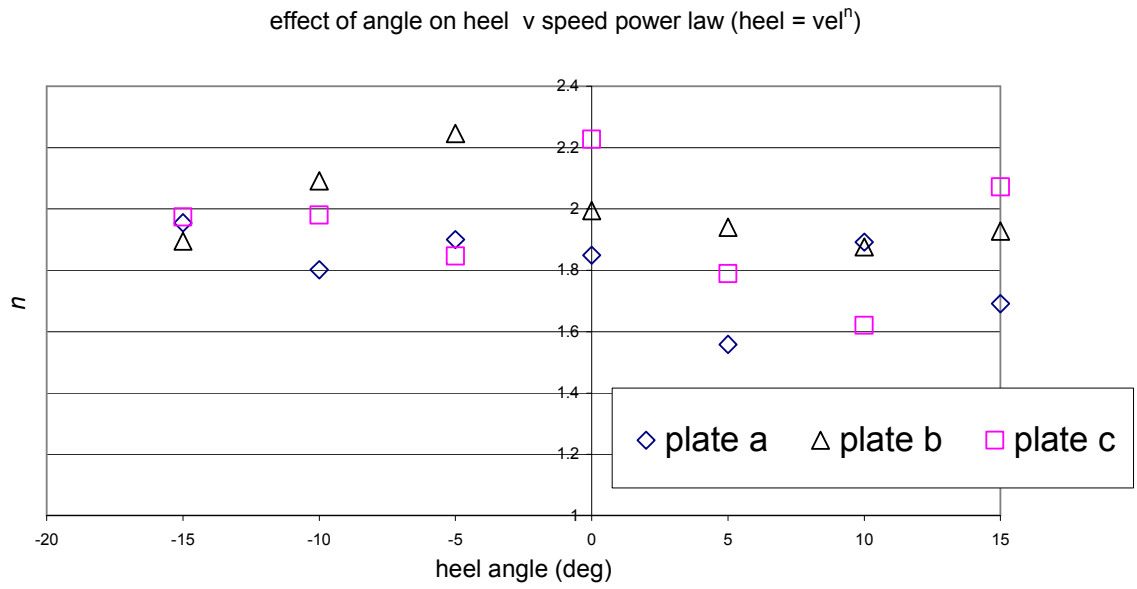

Figure 12 Heel moment power law variation for plate b

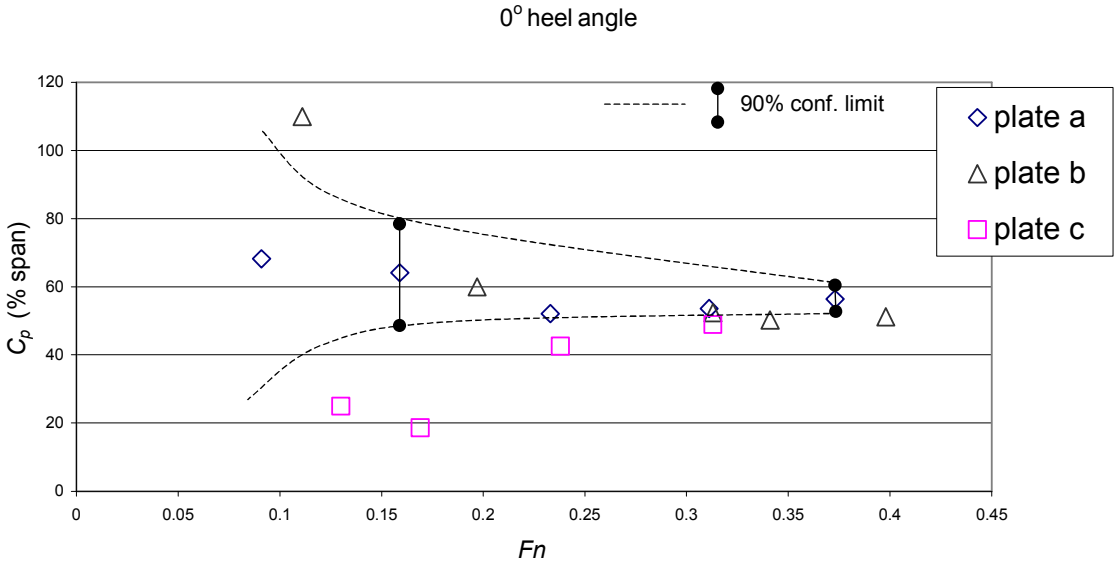

Figure 13 Spanwise centre of pressure at 0° heel angle